Eur Biophys J (2011) 40:1–12
DOI 10.1007/s00249-010-0623-x

ORIGINAL PAPER

The role of aromatic side-chains in amyloid growth and membrane interaction of the islet amyloid polypeptide fragment LANFLVH

Danilo Milardi · Michele F. M. Sciacca · Matteo Pappalardo · Domenico M. Grasso · Carmelo La Rosa

Received: 21 April 2010 / Revised: 27 July 2010 / Accepted: 6 August 2010 / Published online: 1 September 2010

Abstract Human islet amyloid polypeptide (hIAPP) is known to misfold and aggregate into amyloid deposits that may be found in pancreatic tissues of patients affected by type 2 diabetes. Recent studies have shown that the highly amyloidogenic peptide LANFLVH, corresponding the N-terminal 12–18 region of IAPP, does not induce membrane damage. Here we assess the role played by the aromatic residue Phe in driving both amyloid formation and membrane interaction of LANFLVH. To this aim, a set of variant heptapeptides in which the aromatic residue Phe has been substituted with a Leu and Ala is studied. Differential scanning calorimetry (DSC) and membrane-leakage experiments demonstrated that Phe substitution noticeably affects the peptide-induced changes in the thermotropic properties of the lipid bilayer but not its membrane damaging potential. Atomic force microscopy (AFM), ThT fluorescence and Congo red birefringence assays evidenced that the Phe residue is not required for fibrillogenesis, but it can influence the self-assembling kinetics. Molecular dynamics simulations have paralleled the outcome of the experimental trials also providing informative details about the structure of the different peptide assemblies. These results support a general theory suggesting that aromatic residues, although capable of affecting the self-assembly kinetics of small peptides and peptide-membrane interactions, are not essential either for amyloid formation or membrane leakage, and indicate that other factors such as β-sheet propensity, size and hydrophobicity of the side chain act synergistically to determine peptide properties.

Keywords Islet amyloid polypeptide · Differential scanning calorimetry · Membranes · Fibrils · Diabetes mellitus type II

D. Milardi
Istituto di Biostrutture e Bioimmagini, U.O.S. Catania, Consiglio Nazionale delle Ricerche, Viale Andrea Doria 6, 95125 Catania, Italy

M. F. M. Sciacca · M. Pappalardo · D. M. Grasso · C. La Rosa (✉)
Dipartimento di Scienze Chimiche, Universita' di Catania, Viale Andrea Doria 6, 95125 Catania, Italy
e-mail: clarosa@unict.it

Introduction

Human islet amyloid polypeptide (hIAPP) is a peptide hormone consisting of 37 amino acid residues cosecreted with insulin by pancreatic islet β-cells (Cooper et al. 1987; Westermark et al. 1986, 1987a, b). In patients affected by type 2 diabetes mellitus (T2DM), hIAPP aggregates in vivo in the islet extracellular space to form β-sheet rich fibrillar amyloid deposits which are known to be toxic to β-cells (Betsholtz et al. 1989; Clark et al. 1987; Higham et al. 2000; Westermark et al. 1987c). Although the molecular mechanism of hIAPP amyloidogenesis in vivo is not fully understood, the in vitro mechanism has been studied extensively. It has been recently shown that a conformational transition of soluble hIAPP into β-sheets precedes in vitro hIAPP insolubilization into fibrils (Kayed et al. 1999) and that the kinetics of hIAPP amyloid formation are consistent with the nucleation-dependent self-assembling mechanism (Jarrett and Lansbury 1993; Kayed et al. 1999). The exact mechanism of hIAPP toxicity to β-cells is not known but accumulating evidence suggests that it might be related to the hIAPP-induced damage of natural lipid membranes (Anguiano et al. 2002; Konarkowska et al. 2006). Dissecting the properties of different hIAPP sequences is believed to be an effective strategy for

identifying the molecular features driving amyloid fibrils formation, membrane activity and, eventually, toxicity. To this aim, several groups have focused their attention on the different domains contained within the hIAPP sequence and their possible contributions to amyloid formation (Goldsbury et al. 2000; Jaikaran et al. 2001; Nilsson and Raleigh 1999; Tenidis et al. 2000).

In particular it has been demonstrated the presence of an amyloidogenic segment contained within the conserved sequence encompassing residues 8–20 (Jaikaran et al. 2001; Brender et al. 2007). This fragment has also been shown to self-assemble into β-sheet fibrils that are morphologically similar to amyloid observed in vivo (Jaikaran et al. 2001). More recently the N-terminal 1–19 region of hIAPP has been shown to cause extensive membrane damage without forming amyloid fibers (Brender et al. 2008). Computational studies confirmed the high propensity towards ordered β-aggregation of the region encompassing residues 8–20: in particular the segment 12–18 (LANFLVH) has been shown to possess the highest propensity to aggregate into ordered β-sheets of the entire hIAPP sequence (Cecchini et al. 2006). A peptide fragment corresponding to LANFLV (residues 12–17) was shown to be a strong enhancer of β-sheet transition and fibril formation in full-length hIAPP. Moreover, negative stain electron microscopy illustrated the ability of this peptide to form fibrils independently when incubated alone in solution (Scrocchi et al. 2003). While LANFLV was able to enhance the recruitment of additional hIAPP molecules during fibril formation, the ''seeding'' activity of these peptides had no effect on altering hIAPP-induced cytotoxcity as determined by cell culture studies (Scrocchi et al. 2003). Several papers have focused their attention on the His 18 residue showing its ability in both hIAPP fibrillogenesis and membrane interaction (Nanga et al. 2008, 2009). In a recent work some of us have demonstrated that the high fibrillogenic potential of LANFLVH is not paralleled by an evident membrane interaction, thus supporting the hypothesis that mature fibrils are inert by-products and that fibrillogenesis and membrane damage are not necessarily linked by a causative relationship in agreement with other recent reports (Sciacca et al. 2010; Brender et al. 2008).

In an attempt to gain details on the molecular determinants of the biophysical behavior of these amyloidogenic peptides, in the present work we examine the role of the aromatic residue Phe in affecting the fibrillogenic propensity and membrane activity of the peptide LANFLVH. In fact, based on the evidence that this sequence has shown the highest fibrillogenic potential of the whole hIAPP sequence it may be considered as a trustworthy candidate to investigate the role of aromatic residues in modulating the biophysical properties of amyloidogenic peptides. Indeed, some experimental studies suggest that interactions between aromatic residues play a key role in fibril formation by polypeptides (Azriel and Gazit 2001; Gazit 2002b; Mazor et al. 2002; Reches et al. 2002). In contrast, strategies for predicting the intrinsic effects of mutations on the rate of aggregation of unstructured polypeptides have been reasonably successful without including aromatic-aromatic interactions (Chiti et al. 2003). Physicochemical studies using peptide model systems indicate that aromatic residues also have a high tendency to partition into the membrane-water interface (Wimley and White 1996). Here, we test the importance of aromatic–aromatic interactions in amyloid formation and peptide-induced membrane damage in more detail by examining a set of variant peptides derived from the 12–18 region of human IAPP are reported in Fig. 1. In particular, the consequences of substituting the single aromatic residue by Leu and Ala are examined.

Our studies indicate that aromatic–aromatic interactions are not required either for amyloid formation or membrane damage. In agreement with previous data (Tracz et al. 2004), our results confirm that aromatic-aromatic interactions play a role in the kinetics of peptides self-assembling.

Materials and methods

Chemicals

Full length hIAPP, the N-acetylated and C-amidated fragments of human amylin $hIAPP_{21–27}$, $hIAPP_{12–18}$ and its F15L and F15A mutants were purchased from Genscript corporation with a purity of ≈98%; 1,2-dimyristoyl-sn-glycero-3-phosphocholine (DMPC) was purchased from Avanti Polar Lipids, with a purity of ≈98% and used without further purification; 1,1,1,3,3,3-hexafluoro-2-propanol (HFIP), 6-carboxyfluorescein, thioflavin T (ThT), Congo red, $NaH_2PO_4{\cdot}7H_2O$ and $Na_2HPO_4{\cdot}H_2O$ used for buffer preparation were purchased from Sigma–Aldrich, with a purity, at least, of 99%. Before use, peptides were dissolved in HFIP (1.5 mg/ml) to break up any preformed aggregates present in the solution. Aliquots of the peptide stock solution were rotoevaporated under a nitrogen flow for more than 1 h at less than 1 mTorr vacuum to completely remove HFIP leaving a transparent film of peptide

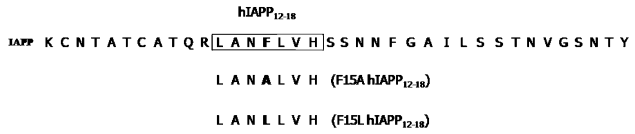

Fig. 1 Primary sequence of hIAPP. Residues from 12 to 18 are closed in a *box*. The two F15A and F15 variants of the peptide $hIAPP_{12–18}$ are also reported

on the internal surface of the tube: next, it was dissolved in the buffer or, alternatively added to lipid dispersions up to the desired lipid/peptide molar ratio (Grasso et al. 2001). The same phosphate buffer was used throughout all the experiments.

Preparation of model membranes

Model membranes were prepared as described elsewhere (Grasso et al. 2001). Briefly, solutions of DMPC in $CHCl_3$ were dried under a nitrogen flow and evaporated under high vacuum to dryness in round-bottomed flasks. The resulting lipid film was hydrated with an appropriate volume of phosphate buffer (10 mM, pH = 7.4) and dispersed by vigorous stirring in a water bath set at 4°C above the gel–liquid crystal transition temperature of the membrane. The final nominal concentration of the lipid was 200 μM. In order to obtain large unilamellar vesicles (LUVs), the multilamellar vesicles were extruded through polycarbonate filters (pore size ≈ 100 nm) (Nuclepore, Pleasanton, CA) mounted in a mini-extruder (Avestin Inc.) fitted with two 0.5 ml Hamilton gastight syringes (Hamilton, Reno, NV). Usually we subjected samples to 23 passes through two filters in tandem as recommended elsewhere (Macdonald et al. 1991). An odd number of passages were performed to avoid contamination of the sample by vesicles which might not have passed through the filter.

ThT fluorescence assays

Fluorescence was monitored as a function of time in a 1 cm path length quartz cuvette by using a Varian Cary Eclipse spectrofluorimeter. Two stock solutions of $hIAPP_{12–18}$ F15L and $hIAPP_{12–18}$ F15A were prepared by dissolving each peptide in 100% HFIP (1.5 mg/ml). Experiments were performed by adding 10 μl of the peptide stock solution into a glass tube. Then, HFIP was removed by a nitrogen stream followed by a vacuum drying for 1 h. The resulting peptide film was then hydrated with 2 ml of phosphate buffer (10 mM, pH 7.4) containing Thioflavin-T (ThT). Final solutions were 20 μM ThT containing 10 μM of peptide. For ThT assays in the presence of membranes, the dry peptide film was hydrated with 2 ml of 200 μM lipid dispersion buffered at pH 7.4 containing ThT. All other experimental conditions are unchanged. All buffer solutions were filtered by using a 0.2 μm filter. The measurements were carried out by using, as a control, the fluorescence versus time curves of ThT solutions without the peptide. The excitation and emission wavelengths were 440 and 481 nm, respectively. Excitation and emission slits values were maintained at 5 and 10 nm, respectively. Spectra were recorded at 10 min intervals for about 24 h, and all measurements were replicated three times. The measurements were carried out in a thermostated room at 27°C under quiescent conditions.

AFM measurements

Peptide aggregates were dried on freshly cleaved mica for 10 min at ambient temperature, washed with 1 ml milli Q water and dried for 20 min. Fibrils morphology was investigated by stomic gorce microscopy (AFM) on a multimode nanoscope IIIA (Digital Instruments, Santa Barbara, USA) with a 10-μm scanner. Sharpened silicon nitride probes with a radius, $r = 30$ nm, and a nominal spring constant, $k = 0.06$ N m^{-1} were employed (Veeco, probes). Tapping mode in air imaging was performed by using phosphorus (n) doped Si probes.

Congo red staining

Congo red birefringence of the aggregates under cross polarizers was evaluated by an optical Zeiss Axioplan polarizing microscope equipped with a digital camera. Samples were prepared by adding 1 μl of a hydroalcoholic solution of Congo red to 3 μl of buffer solutions of the peptide. Glass slices so prepared were dried in air for 6 h Images were acquired after 20 h under bright field illumination and then between crossed polarizers at 50 × magnification in order to evaluate the presence of amyloid fibrils. The measurements were carried out in a thermostat-controlled room at 27°C.

Membrane leakage experiments

Membrane leakage experiments were carried out by using 6-carboxyfluorescein-filled LUVs of DMPC (200 μM). Dye-filled DMPC LUVs were prepared by hydrating the dry lipid film with the buffer solution containing 6-carboxyfluorescein (0.1 M) according to the procedure described above. After the extrusion, LUVs were dialyzed overnight at $T = 20$°C through a membrane with a cut-off of 2,000 Da in order to eliminate the dye not encapsulated into LUVs. Leakage experiments were started by adding an aliquot of peptide stock solution to an empty glass tube. Next, organic solvent was evaporated by using a gentle stream of dry nitrogen followed by vacuum desiccation for 1 h. The resulting peptide film was then dissolved into dye-filled DMPC LUVs. Membrane damage was quantified by detecting the increment of fluorescence emission intensity of 6-carboxyfluorescein due to its dilution (dequenching) in buffer as a consequence of the membrane leakage. All spectra were corrected by subtracting a baseline obtained as the signal detected prior to the addition of the peptide solution. The excitation and emission wavelength was 490 and 515 nm, respectively. Excitation and emission slits

were maintained at 5 and 10 nm, respectively. Spectra were recorded at 30 min intervals for 24 h. All measurements are an average of three replicated experiments. The maximum leakage at the end of each measurement was determined by adding 2 μl of 10% Triton X-100 to a final concentration of 0.1% (vol/vol). The release percentage of the fluorescent dye (membrane leakage) was calculated according to the equation: % release $= (I - I_0)/(I_{100} - I_0)$, where I is the fluorescence intensity at 515 nm of the sample, I_0 is the fluorescence at 515 nm in the absence of peptides and I_{100} is the fluorescence intensity after the addition of Triton X-100. The measurements were carried out in a thermostated room at 27°C under quiescent conditions.

Differential scanning calorimetry (DSC)

DSC runs of DMPC LUVs were carried out on a VP-DSC (MicroCal) apparatus. All the lipid samples were degassed by vacuum and then heated from 10 to 50°C at a scan rate of 1°C min^{-1}. Preliminary trials have shown that a 10 μM peptide concentration and a 200 μM lipid concentration in a 10 mM phosphate buffer pH = 7.4 represent the best compromise between stability of lipid vesicles, solubility of peptides and instrumental sensitivity. Consequently, a peptide/lipid ratio 20:1 was used in all the experiments. An extra external pressure of about 2 bar was applied on the solution to prevent the formation of bubbles during heating. The buffer solution was used as the reference. Heat capacity curves (Cp), were obtained by subtracting the buffer–buffer baseline from raw DSC data. All DSC runs were performed immediately after the preparation of samples and after 20 h in order to observe if kinetic effects are present. The results of DSC experiments were the average of three different scans.

Molecular dynamics

Constant temperature molecular dynamics (CT-MD) simulations of N-acetylated and C-amidated $hIAPP_{12–18}$ F15L and F15A were performed with the program CHARMM33 (Brooks et al. 1983; Gsponer et al. 2003; Neria et al. 1996). All peptide systems were modeled by explicitly considering all heavy atoms and the polar hydrogen atoms bound to nitrogen and oxygen. The CHARMM 19 potential function was adopted and default cutoffs for long range interactions were used, i.e. a shift function (Fernandez-Escamilla et al. 2004) of 1 Å was employed with a cut-off at 7.5 Å for both the electrostatic and van der Waals terms. Langevin dynamics with a friction value of 0.15 ps^{-1} were used (Cecchini et al. 2006). The solvent was simulated by adopting an implicit water model (EFF1) widely tested (Lazaridis and Karplus 1999a, b). In order to implicitly mimic the lipid bilayer, we adopted the IMM1 extension of EFF1 (Lazaridis 2003). The hydrocarbon core of a DMPC membrane is simply defined as a plane with a thickness of 23.1 Å embedded in a medium with implicit water. The SHAKE algorithm (Brooks et al. 1983) was used to fix the length of the covalent bonds involving hydrogen atoms, and an integration time step of 2 fs, was used. Furthermore, the non-bonded interactions were updated every ten dynamics steps and the coordinate frames were saved every 20 ps. A 20 ns implicit water MD simulation was performed on each single heptapeptide at $T = 300$ K to equilibrate the monomer. For each heptapeptide, three replicas of the equilibrated monomer were used to simulate the early steps of aggregation in water and in a membrane-like environment. In the initial positions there were neither inter- nor intramolecular contacts: i.e. the three peptides were completely unfolded and not interacting in space. All simulations were started from random positions, orientations and conformations of the peptide copies. When the implicit membrane was introduced, the initial position of the mass center of one heptapeptide was chosen in the center of the bilayer; the mass centers of the other two replicas were located 20 Å far away the membrane surface on the two opposite sides of the membrane. The final three-meric assembly was simulated in a cubic box of 186 Å side and re-equilibrated for 20 ns at 300 K. Next, productive MD simulations were carried out at 300 K for overall 2 μs. Implicit membrane MD simulations were paralleled by simulations in water in which all the other parameters were not changed. The nematic order parameter $\overline{P_2}$ was considered to monitor the aggregation process as described elsewhere (Cecchini et al. 2006). This order parameter is widely used to study the properties of anisotropic fluids (Cecchini et al. 2004) and is defined as:

$$\overline{P_2} = \frac{1}{N}\sum_{i=1}^{N}\frac{3}{2}\left(\overrightarrow{z_1} \times \overrightarrow{d}\right)^2 - \frac{1}{2}$$

where $\overrightarrow{d}$ (the director) is a unit vector defining the preferred direction of alignment, $\overrightarrow{z_i}$ are the molecular unit vectors linking the peptide's N- and C-termini and N is the number of molecules in the simulation box, i.e. three in the present study. The order parameter $\overline{P_2}$ describes the orientational order of the system and discriminates between ordered and disordered conformations. $\overline{P_2}$ values close to the unity represent highly ordered aggregates while values close to 0.5 represent disordered systems.

Results

Membrane interaction of $hIAPP_{12–18}$ and its F15L and F15A variants

It is widely acknowledged that DSC is an important tool to investigate the peptide-induced perturbation of lipid

bilayers (Sciacca et al. 2008): in fact the heat-capacity (Cp) changes concerning the main transition of lipid/peptide systems may help to clarify not only the effects of the presence of the peptide on the physical state of the membrane, but also the topological arrangement of the peptide inserted into a lipid matrix. Indeed, the enthalpy change (ΔH) observed during the lipid main transition is mainly ascribable to the packing efficiency of the hydrocarbon tails (Grasso et al. 2001). The peptide-induced decrease of the transition enthalpy of the bilayer may, thus, be related to the extent of the interaction between guest molecules and the hydrocarbon core of lipid membranes. The temperature at which the main transition occurs, T_m, is more sensitive to interactions involving the lipid head groups, and changes when the membrane surface is involved in the interaction with the guest peptide (Grasso et al. 2005; Sciacca et al. 2008). Moreover, membrane binding of peptides is known to induce negative or positive curvature strain on the membrane depending on the nature of lipid-peptide interactions (Matsuzaki et al. 1998). The phase transition temperature is often measured to assess this curvature stress exerted on the membrane (Ramamoorthy et al. 2006). In particular a decrease in T_m consequent to peptide addition suggests that the vesicles are destabilized by the negative strain of the lipid bilayer (Smith et al. 2010). Figure 2 shows the Cp profiles of large unilamellar vesicles (LUVs) of 20:1 DMPC/hIAPP$_{12–18}$, DMPC/F15LhIAPP$_{12–18}$ and DMPC/F15AhIAPP$_{12–18}$, compared with the Cp profile of pure DMPC. To evidence possible kinetic effects, DSC runs of the lipid/peptide mixtures were performed immediately after the addition of the peptide to LUVs (solid lines) and repeated after 20 h of incubation (dotted lines). All the relative calorimetric data are collected in Table 1.

The effect of the peptides on the phase behavior of DMPC LUVs immediately after its addition to the lipid dispersion ($t = 0$ h) is evidenced by a significant decrease of the temperature of the main transition. DSC runs repeated after 20 h on the same samples show that the peptide-induced membrane interaction are almost time-independent. In fact the enthalpy change associated with the thermal transition of DMPC LUVs incubated for 20 h with hIAPP$_{12–18}$ F15L is lower than samples scanned immediately after peptide addition. The peptide-induced decrease of both T_m and ΔH is ascribable to the insertion of the peptide into the hydrocarbon core of the bilayer (Nanga et al. 2008) however because of the small decrease in ΔH we deduce that the peptide interacts mainly with the surface of LUVs, as also evidenced by the high decrease of the transition temperature. Conversely, the interaction of hIAPP$_{12–18}$ F15A with DMPC LUVs induced a decrease in T_m and only weak decrease of ΔH. These effects are time-independent because the DSC curve relative to the lipid bilayer incubated for 20 h with hIAPP$_{12–18}$ F15A is similar

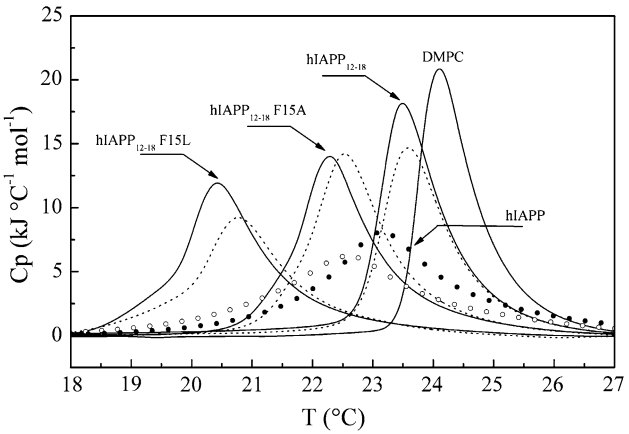

Fig. 2 Heat-capacity profiles (Cp) of LUVs of 20:1 DMPC/hIAPP$_{12–18}$, DMPC/hIAPP$_{12–18}$ F15L, and DMPC/hIAPP$_{12–18}$ F15A obtained immediately after peptide addition to the lipid dispersion (*solid lines*) and after 20 h of incubation (*dotted lines*). The Cp profile of pure DMPC LUVs is also reported for comparison. The effect of full-length hIAPP on the phase behavior of DMPC LUVs observed immediately after peptide addition (*closed circles*) and after 20 h of incubation (*open circles*) is shown. Experimental conditions were the same as for the short fragments

Table 1 Calorimetric parameters ΔH and T_m relative to the main transition of different peptide/lipid LUVs systems at different times of peptide incubation prepared as reported in the Experimental Section

Lipid/peptide system	Incubation time, t (h)	T_m (°C)	ΔH (kJ mol^{-1})
DMPC		24.1 (0.1)	27.2 (1.4)
DMPC + hIAPP	0	23.1 (0.1)	24.5 (1.2)
DMPC + hIAPP	20	22.5 (0.1)	21.7 (1.2)
DMPC + hIAPP$_{12–18}$	0	23.4 (0.1)	27.1 (1.3)
DMPC + hIAPP$_{12–18}$	20	23.7 (0.1)	22.4 (1.3)
DMPC + hIAPP$_{12–18}$ F15L	0	20.4 (0.1)	22.6 (1.2)
DMPC + hIAPP$_{12–18}$ F15L	20	20.2 (0.1)	20.7 (1.0)
DMPC + hIAPP$_{12–18}$ F15A	0	22.3 (0.1)	25.0 (1.3)
DMPC + hIAPP$_{12–18}$ F15A	20	22.5 (0.1)	25.0 (1.3)

DSC parameters of pure DMPC were not modified after 20 h of incubation. The reported values are the mean of three repeated experiments. Standard deviations are reported in parentheses

to the peak recorded by scanning a freshly prepared lipid/peptide mixture. In an previous set of experiments carried out on a series of peptides Ala-X-Ala-O-tert-butyl (X = Trp, Phe, Leu, Ala, Gly), the free energy for partitioning of the peptides into the bilayer decreases from −5.12 kcal/ml for Trp to −2.91 kcal/ml for Gly (Jacobs and White 1986). This difference is ascribable to the different hydrophobic interactions between the lipid alkyl region and the central side chain. In apparent contrast with these data our results suggest that the replacement of Phe with Ala or Leu residues increases the potential of the peptide to interact with the membrane. It is, thus,

conceivable that other factors, e.g. an enhanced ability of the peptide to self assemble through aromatic–aromatic interactions, could interfere with the peptide partitioning into the membrane. Notably, the effect of the full-length hIAPP on the phase behavior of DMPC is not different from the three heptapeptides. The percentage release of the fluorescent dye, 6-carboxyfluoresceine, from DMPC LUVs (Fig. 3) was monitored to evidence the peptide-induced membrane damage as a function of time. Figure 3 shows that both the F15L and F15A did not cause appreciable dye release from DMPC vesicles. These results suggest that the negative curvature strains exerted by the peptides in lipid bilayers, as inferred by DSC peaks, are not sufficient to induce membrane disruption.

Thioflavine-T (ThT) assays of $hIAPP_{12–18}$ and $hIAPP_{21–27}$ fibril growth in buffer and membranes

Figure 4 reports ThT fluorescence assays of full length hIAPP, $hIAPP_{12–18}$ and its F15A, F15L variants in buffer (upper panel) and in the presence (lower panel) of zwitterionic membranes. In all cases the peptides induced increment in fluorescence emission after addition to a freshly prepared ThT solution. In water, $hIAPP_{12–18}$ exhibited a sigmoidal growth of ThT fluorescence as a consequence of amyloid-like fibril formation. The F15A peptide evidenced a decrease in the rate of fibril formation. A comparison of membrane leakage experiments with ThT fluorescence data pointed out that $hIAPP_{12–18}$ F15A has a remarkable propensity to aggregate in amyloid-like structures but does not cause membrane damage; in membranes, the peptide is less prone to form fibrillar aggregates, as shown by the lower intensity of fluorescence emission. Moreover, in the presence of membrane a lag time of about 200 min before aggregation was observed.

In absence of membranes $hIAPP_{12–18}$ F15L rapidly increases ThT fluorescence emission, due to its high propensity to form amyloid fibrillar aggregates. After about 250 min ThT fluorescence emission intensity decreases exponentially, probably because of the precipitation of the newly formed fibrillar aggregates. A similar behavior was observed in presence of membranes (Fig. 4 open circles), but with some significant differences: (a) the formation of fibrils is less rapid, as evidenced by $t_{1/2}$ about 150 min in absence of membrane versus 350 min in presence of phospholipid bilayer; (b) the propensity to form fibrils is less pronounced as shown by the lower fluorescence intensity; (c) the precipitation of the system is less evident. Even in the case of $hIAPP_{12–18}$ F15L, if one compares ThT assays with membrane leakage experiments it may be observed that in spite of amyloid fibrils formation propensity, there are no evidences that this peptide may induce membrane damage.

AFM and Congo red staining assays

The amyloid-like structure of the peptides aggregates was observed by AFM and optical anisotropy after treatment

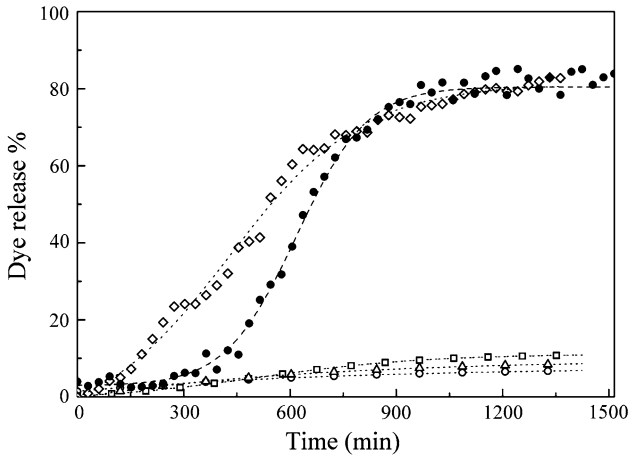

Fig. 3 Dye release—normalized membrane leakage versus time measured after the addition of $hIAPP_{12–18}$ (*square*), F15A (*triangle*), F15L (*open circle*) to DMPC membranes. The membrane leakage profiles of hIAPP (*filled circle*) and $hIAPP_{21–27}$ (*diamond*) are reported for comparison. All peptides were added at a concentration of 10 μM to dye filled DMPC LUVs (200 μM lipids)

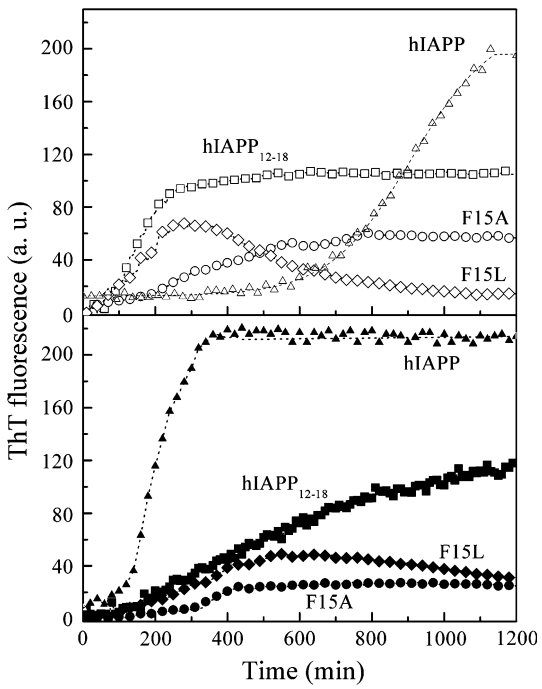

Fig. 4 *Upper panel* ThT fluorescence emission profiles versus time of hIAPP (*open triangle*), $hIAPP_{12–18}$ (*open square*) and its F15A (*open circle*) and F15L (*open diamond*) variants in buffer solution. *Lower panel* ThT fluorescence emission profiles versus time of hIAPP (*filled triangle*), $hIAPP_{12–18}$ (*filled square*) and its F15A (*filled circle*) and F15L (*filled diamond*) in DMPC membranes

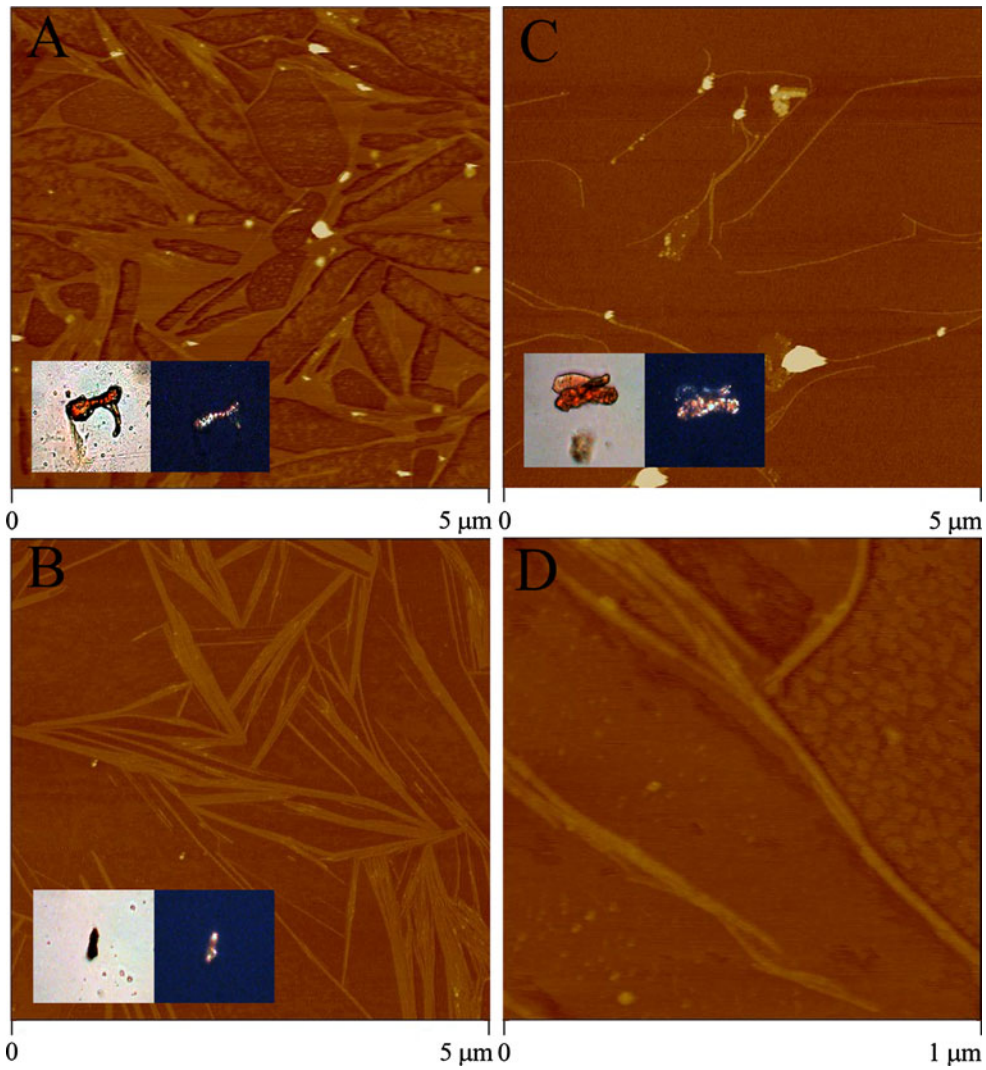

Fig. 5 AFM images of $hIAPP_{12\text{-}18,}$ (**a**), $hIAPP_{12–18}$ F15L (**b**) and $hIAPP_{12–18}$ F15A (**c**). A ×5 magnification of a representative region of **a** is reported in **d**. The amyloid-like nature of the aggregates was further evidenced by optical birefringence assays after treatment with a Congo red/ethanol solution (*insets*). All the images were obtained after 20 h of incubation at room temperature

with Congo red/ethanol solution. In Fig. 5 some representative AFM images and optical anisotropy relative to the three heptapeptides are shown. In particular, panels A, B and C show the morphology of $hIAPP_{12–18}$, $hIAPP_{12–18}$ F15L and $hIAPP_{12–18}$ F15A fibrils peptide and their optical anisotropy (left inset: normal mode; right inset: polarized mode), respectively. As expected, although all aggregates showed in Fig. 5 were obtained in the same experimental conditions, their morphology was very different. In fact, $hIAPP_{12–18}$ formed the largest fibrillar aggregates as shown in Fig. 5 panel A and in its magnification (Fig. 5, panel D). On the other hand, $hIAPP_{12–18}$ F15A formed few spaghetti-like aggregates, and finally $hIAPP_{12–18}$ F15L showed an intermediate situation in agreement with ThT fluorescence data.

Implicit solvent molecular dynamics simulation of $hIAPP_{12–18}$ F15L and $hIAPP_{12–18}$ F15A aggregation in water and in DMPC membranes

Molecular dynamics simulations of peptide aggregation in water and in membrane-like environments are expected to complement the experiments by providing atomistic details concerning the structure of the aggregates and the topology of their assembly with the lipid bilayer. In particular, the morphology of the aggregates (ordered or amorphous) and the extent of insertion into the lipid matrix may provide fundamental clues concerning the nature of the lipid-peptide interactions. To this aim, we monitored the propensity of $hIAPP_{12–18}$ and its F15L or F15A variants to form ordered aggregates in water and in membrane by plotting

the nematic order parameter P_2 calculated from the analysis of the frames over 2 μs MD (Fig. 6). As previously reported (Sciacca et al. 2010), in water $hIAPP_{12–18}$ has a high propensity to self-assemble into ordered aggregates ($P_2 = 0.83$), in agreement with previously reported data (Cecchini et al. 2006). However, a small shoulder centered at $P_2 = 0.46$ indicates the persistence of a little percentage of amorphous aggregates which may be ascribed to an equilibrium existing between ordered and disordered aggregates. A parallel set of simulations carried out in implicit membrane shows a sharp peak centered at $P_2 = 0.48$ suggesting that the membrane has an effective disordering effect on the peptide aggregates. If compared to $hIAPP_{12–18}$, the F15L variant exhibits in water a slightly lower propensity to self-assemble into ordered aggregates ($P_2 = 0.72$).

A parallel set of simulations carried out in implicit membrane showed a little decrease of the nematic order parameter ($P_2 = 0.75$) suggesting a small disordering effect of the membrane environment for $hIAPP_{12–18}$ F15L. The presence of two peaks centered at $P_2 = 0.46$ and $P_2 = 0.80$ in the self-assembling of $hIAPP_{12–18}$ F15A in water indicates the persistence of a little percentage of disordered aggregates which may be ascribed to an equilibrium between ordered and disordered aggregates. Notably, a parallel MD simulation carried out in a membrane-like environment exhibited a population of frames with a peaked distribution centered at $P_2 = 0.88$. This means that the most populated system is highly ordered and that the presence of a membrane-like environment acts as a template for an ordered aggregation of $hIAPP_{12–18}$ F15A. These findings reconcile with recent experiments suggesting that membrane damage may proceed by aggregation of monomeric hIAPP on the membrane rather than the insertion of preformed structured oligomers from the solution state (Soong et al. 2009). The affinity of the different peptide aggregates for the membrane-like was established by plotting the number of frames as a function of their position along the Z direction of the lipid bilayer (Fig. 7). It was evidenced that the three-meric aggregates of both mutant of the $IAPP_{12-18}$ were mainly located at $Z = +13$ Å and $Z = -13$ Å in the external zone of the lipid bilayer were electrostatic forces are predominant with respect to the hydrocarbon core. Conversely, the aggregates of $hIAPP_{12–18}$ are located in the outer zone of the membrane surface with respect to its two mutants ($Z = \pm 22$ Å).

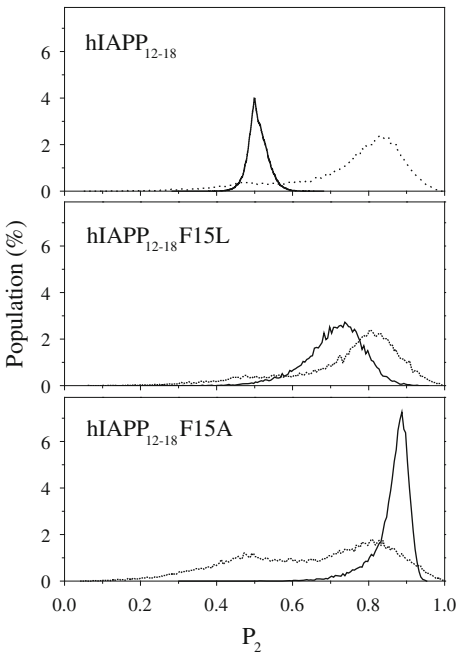

Fig. 6 Populations versus the total number of frames of $hIAPP_{12–18}$, $hIAPP_{12–18}$ F15L, and $hIAPP_{12–18}$ F15A aggregates along the $\overline{P_2}$ order parameter calculated from MD simulations performed in implicit membrane (*solid lines*) and water (*dotted line*). All simulations were performed at $T = 300$ K for 2 μs. The values on the *y*-axis are normalized so that the area under each peak represents the unity

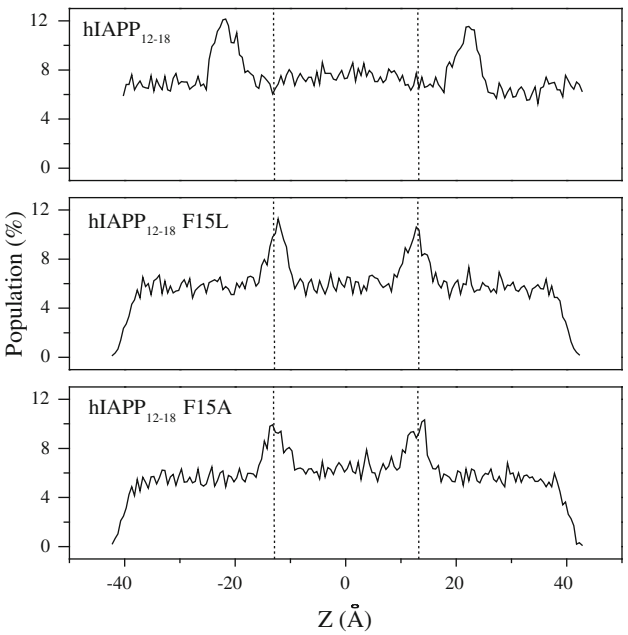

Fig. 7 One-dimensional distribution of populations of the three-meric aggregates of $hIAPP_{12–18}$ and its variants F15L and F15A along the director (z-axis) of the DMPC lipid bilayer calculated from the analysis of the frames extracted from 2 μs implicit-membrane MD simulations at $T = 300$ K. *Dotted lines* represent the membrane boundaries

Discussion

Elucidating the specific interactions and patterns of residues that stabilize amyloid fibrils and guide their self-assembly and/or membrane interaction is a key step in

developing strategies to inhibit and control amyloid toxicity (Broome and Hecht 2000; Chiti et al. 2003; de la Paz and Serrano 2004; Mazor et al. 2002).Of particular interest are the interactions involving aromatic rings, which are proposed to regulate the geometry of closely packed peptide assemblies. In fact, such interactions reflect the electrostatic contribution of π-electrons and, unlike van der Waals' interactions and the hydrophobic effect may, in principle, introduce a directional force in peptide aggregation (Burley and Petsko 1985, 1986, 1988). Although the general importance of such contributions to amyloid assembly has been already discussed (Gazit 2002a, b), their concomitant role in driving the membrane interactions of the peptide aggregates is still unclear. The classical description of peptide partitioning in membrane provides a quantitative evaluation of the energetic cost of transferring a peptide from water into the membrane (Wimley and White 1996). Because of the unfavorable energetic cost of transferring a peptide bond into the interior of the membrane small peptides that are supposed to lack well defined secondary structure are likely to interact only with the interface region of the membrane (Wimley and White 1996). According to this description aromatic residues are found to be especially favored to lie at the membrane interface. Instaed, Phe, Leu and Ala residues (Phe > Leu > Ala) have shown a high propensity to partition into the membrane interface. In apparent contrast with this hydropathy scale DSC data reported here demonstrate that the $hIAPP_{12–18}$ peptide has the lowest propensity to interact with the membrane while its F15L variant has the highest potential to perturb the thermotropic properties of the membrane. To explain this apparent contradiction it should be reminded that the principal design criteria for model peptides used in the measurement of water-membrane partition coefficients were that peptides be soluble in water as monomers. This means that these models do not take into account the ability to these peptides to self-assemble into intermolecular aggregates and underestimate the competing role played by aggregation versus membrane partitioning. In a previous work some of us have demonstrated that the highly fibrillogenic peptide $hIAPP_{12–18}$, does not affect noticeably the physicochemical properties of zwitterionic membranes, supporting the hypothesis that fibril growth is not an essential pre-requisite to induce membrane-damage (Sciacca et al. 2010). In the same paper MD simulations have demonstrated that $hIAPP_{12–18}$, if embedded in zwitterionic model membranes, has a tendency to form disordered aggregates. The affinity of these aggregates for the hydrophobic core of the membrane is very low and it is also observed that they preferentially lie on the surface of the membrane, in agreement also with the outcome of DSC experiments. Here, a parallel set of experiments carried out on the two F15L and F15A variants of $hIAPP_{12–18}$ demonstrated that the replacement of Phe15 with a Leu, or alternatively, an Ala residue did not abolish the ability of the peptide to form fibrils. These substitutions affected the kinetics of fibrils growth and the ability of the peptide to affect the physicochemical features of the membrane. Importantly, none of the peptides investigated here was able to induce membrane leakage as evidenced by dye-release experiments, confirming once again that although a causative relationship linking amyloid growth and membrane damage has been reported elsewhere (Engel et al. 2008), these two processes may also occur independently, thus supporting the important role played by "off-pathways" intermediate aggregates in triggering membrane leakage (Sciacca et al. 2010). ThT fluorescence assays have shown that the replacements of Phe 15 with Leu or Ala residues decreased the fibril growth kinetics of the $hIAPP_{12–18,}$ thus confirming the important role of aromatic residues in fibrils self-assembling. These results are in good agreement with the β-sheet propensities of Phe, Leu and Ala as judged by statistical surveys and by thermodynamic measurements on model proteins. For example, the statistical β-sheet propensity of Phe is 1.33 using a scale where a value of 1.0 corresponds tono statistical preference to be in a β-sheet (Chou and Fasman 1978; Smith and Regan 1997; Williams et al. 1987). Ala, in contrast, has a low β-sheet propensity of 0.72. The β-sheet propensity of Leu, 1.22, is noticeably higher than that of Ala, although somewhat smaller than Phe. Although some precipitation affected the ThT fluorescence of the F15L variant, the relative rates of fibril growth are in agreement with the trend of β-sheet propensities of the three residues (Phe > Leu > Ala). The presence of zwitterionic membranes decreased the rate of fibril growth for all the three peptides challenging the traditional view of membranes as catalysts of amyloid aggregation (Knight and Miranker 2004). More recently, this view has been also questioned by experimental and computational studies in which soluble species were observed upon fibril degradation induced by lipid vesicles (Friedman et al. 2010; Martins et al. 2008). While interpreting the details of these seemingly mutually exclusive models, it is important to note that most studies have been performed under experimental conditions that differed somewhat with respect to lipid composition, buffer solutions, and sample preparation. Thus, it might be possible that fibrils can interact with membranes in a variety of ways depending especially on lipid composition. Our results reconcile with a view in which a zwitterionic lipid vesicle is attractive to peptide hydrophobic residues: this would imply that membrane interactions and peptide-peptide interactions are two competing reactions whose kinetics may be driven by a delicate balance of hydrophobic/electrostatic forces. MD simulations have confirmed a preferential interaction of the F15L and

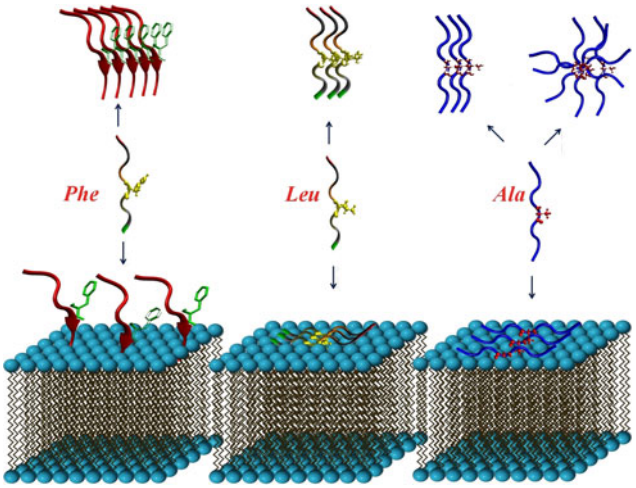

Fig. 8 Schematic representation of the two competing processes involving peptides in water/membrane environments: peptide–peptide self assembling and peptide partitioning in the membrane. The presence of the zwitterionic membrane interferes with the ordered peptide aggregation driven by aromatic–aromatic interactions

F15A variants for the interfacial region of the membrane in agreement with thermodynamic models (Wimley and White 1996). A comparison of the nematic order parameters P_2 of $hIAPP_{12–18}$ calculated in water and in a membrane-like environment revealed that the formation of highly ordered aggregated structures could be severely perturbed by the membrane. This observation supports the hypothesis that the hydrophobic environment provided by the membrane would interfere with a directional peptide aggregation by competing for aromatic side-chains. This effect is much less evident for the F15L variant in agreement with a lower affinity of Leu for the membrane. Conversely, the presence of the membrane induced the formation of ordered F15A $hIAPP_{12–18}$ aggregates, thus suggesting that in this case the balance between hydrophobicity, steric hindrance and β-sheet propensity makes the membrane interface a suitable template for peptide ordered aggregation. The competition between membrane partitioning and self-assembling for the three peptides, $hIAPP_{12–18}$, $hIAPP_{12–18}$ F15L and $hIAPP_{12–18}$ F15A is summarized schematically in Fig. 8.

Conclusion

This work demonstrates that the aromatic residue Phe at position 15 is not essential for amyloid formation by C and N-terminally blocked peptides derived from the 12–18 region of hIAPP. The aromatic ring, however, may affect the kinetics of self-assembling by providing a directional force in peptide–peptide interactions, thus facilitating the formation of highly ordered aggregates. Because of the high affinity of Phe for the interfacial region of lipid bilayer, the presence of the membrane interferes with aromatic-aromatic interactions and decreases the rate of fibril growth. Our results reconcile with a scenario in which aggregation and membrane interactions are two competing reactions whose relative rates are determined by a number of parameters as residue β-sheet propensity, hydrophobic/electrostatic character and size.

Acknowledgments This work was financially supported by Università degli Studi di Catania and CNR (grant RSTL no. 620). We gratefully acknowledge Dr. Graziana Messina and Prof. Giovanni Marletta for their assistance in performing AFM experiments. Molecular Dynamics were performed by using the computational resources of CASPUR (AMD Opteron 50 CPU Linux Clusters).

References

Anguiano M, Nowak RJ, Lansbury PT (2002) Protofibrillar islet amyloid polypeptide permeabilizes synthetic vesicles by a pore-like mechanism that may be relevant to type II diabetes. Biochemistry 41:11338–11343

Azriel R, Gazit E (2001) Analysis of the structural and functional elements of the minimal active fragment of islet amyloid polypeptide (IAPP)—An experimental support for the key role of the phenylalanine residue in amyloid formation. J Biol Chem 276:34156–34161

Betsholtz C, Svensson V, Rorsman F, Engstrom U, Westermark GT, Wilander E, Johnson K, Westermark P (1989) Islet amyloid polypeptide (IAPP): cDNA cloning and identification of an amylodogenic region associated with the species-specific occurrence of age-related diabetes mellitus. Exp Cell Res 183:484–493

Brender JR, Dürr UHN, Heyl D, Budarapu MB, Ramamoorthy A (2007) Membrane fragmentation by an amyloidogenic fragment of human Islet Amyloid Polypeptide detected by solid-state NMR spectroscopy of membrane nanotubes. Biochim Biophys Acta 1768:2026–2029

Brender JR, Lee EL, Cavitt MA, Gafni, Steel DG, Ramamoorthy A (2008) Amyloid fiber formation and membrane disruption are separate process localized in two distinct regions of IAPP, the type-2-diabetes-related peptide. J Am Chem Soc 130:6424–6429

Brooks BR, Bruccoleri RE, Olafson BD, States DJ, Swaminathan S, Karplus M (1983) CHARMM: a program for macromolecular energy, minimization, and dynamics calculations. J Comp Chem 4:187–217

Broome BM, Hecht MH (2000) Nature disfavors sequences of alternating polar and non-polar amino acids: implications for amyloidogenesis. J Mol Biol 296:961–968

Burley SK, Petsko GA (1985) Aromatic-aromatic interaction: a mechanism of protein structure stabilization. Science 229:23–28

Burley SK, Petsko GA (1986) Dimerization energetics of benzene and aromatic amino acid side chains. J Am Chem Soc 108:7995–8001

Burley SK, Petsko GA (1988) Weakly polar interactions in proteins. Adv Protein Chem 39:125–189

Cecchini M, Rao F, Seeber M, Caflisch A (2004) Replica exchange molecular dynamics simulations of amyloid peptide aggregation. J Chem Phys 121:10748–10756

Cecchini M, Curcio R, Pappalardo M, Melki R, Caflisch A (2006) A molecular dynamics approach to the structural characterization of amyloid aggregation. J Mol Biol 357:1306–1321

Chiti F, Stefani M, Taddei N, Ramponi G, Dobson CM (2003) Rationalization of the effects of mutations on peptide and protein aggregation rates. Nature 424:805–808

Chou PY, Fasman GD (1978) Prediction of the secondary structure of proteins from their amino acid sequence. Adv Enzymol 47:45–148

Clark A, Cooper GJS, Lewis CE, Morris JF, Willis AC, Reid KB, Turner RC (1987) Islet amyloid formed from diabetes-associated peptide may be pathogenic in type-2 diabetes. Lancet 2:231–234

Cooper GJS, Willis AC, Clark A, Turner RC, Sim RB, Reid KBM (1987) Purification and characterisation of a peptide from amyloid-rich pancreases of type-2 diabetic patients. Proc Natl Acad Sci USA 84:8628–8632

de La Paz ML, Serrano L (2004) Sequence determinants of amyloid fibril formation. Proc Natl Acad Sci USA 101:87–92

Engel MFM, Khemtémourian L, Kleijer CC, Meeldijk HJD, Jacobs J, Verkleij AJ, de Kruijff B, Killian JA, Höppener JWM (2008) Membrane damage by human islet amyloid polypeptide through fibril growth at the membrane. Proc Natl Acad Sci USA 105:6033–6038

Fernandez-Escamilla AM, Rousseau F, Schymkowitz J, Serrano L (2004) Prediction of sequence-dependent and mutational effects on the aggregation of peptides and proteins. Nat Biotechnol 22:1302–1306

Friedman R, Pellarin R, Caflisch A (2010) Soluble protofibrils as metastable intermediates in simulations of amyloid fibril degradation induced by lipid vesicles. J Phys Chem Lett 1:471–474

Gazit E (2002a) Mechanistic studies of the process of amyloid fibrils formation by the use of peptide fragments and, analogues: Implications for the design of fibrillization inhibitors. Curr Med Chem 9:1725–1735

Gazit E (2002b) A possible role for pi-stacking in the self-assembly of amyloid fibrils. Faseb J 16:77–83

Goldsbury C, Goldie K, Pellaud J, Seelig J, Frey P, Muller SA, Kistler J, Cooper GJS, Aebi U (2000) Amyloid fibril formation from full-length and fragments of amylin. J Struct Biol 130:352–362

Grasso D, Milardi D, La Rosa C, Rizzarelli E (2001) DSC study of the interaction of the prion peptide PrP106–126 with artificial membranes. New J Chem 25:1543–1548

Grasso D, Grasso G, Guantieri V, Impellizzeri G, La Rosa C, Milardi D, Micera G, Osz K, Pappalardo G, Rizzarelli E, Sanna D, Sovago I (2005) Environmental effects on a prion's helix II domain: Copper(II) and membrane interactions with PrP180–193 and its analogues. Chem Eur J 12:537–547

Gsponer J, Haberthur U, Caflisch A (2003) The role of side-chain interactions in the early steps of aggregation: Molecular dynamics simulations of an amyloid-forming peptide from the yeast prion Sup35. Proc Natl Acad Sci USA 100:5154–5159

Higham CE, Jaikaran ETAS, Fraser PE, Gross M, Clark A (2000) Preparation of synthetic human islet amyloid polypeptide (IAPP) in a stable conformation to enable study of conversion to amyloid-like fibrils. Febs Lett 470:55–60

Jacobs RE, White SH (1986) Mixtures of a series of homologous hydrophobic peptides with lipid bilayers: a simple model system for examining the protein-lipid interface. Biochemistry 25:2605–2612

Jaikaran ETAS, Higham CE, Serpell LC, Zurdo J, Gross M, Clark A, Fraser PE (2001) Identification of a novel human islet amyloid polypeptide beta-sheet domain and factors influencing fibrillogenesis. J Mol Biol 308:515–525

Jarrett LL, Lansbury PT Jr (1993) Seeding onedimensional crystallization of amyloid: a pathogenic mechanism in Alzheimer's disease and scrapie? Cell 73:1055–1058

Kayed R, Bernhagen J, Greenfield N, Sweimeh K, Brunner H, Voelter W, Kapurniotu A (1999) Conformational transitions of islet amyloid polypeptide (IAPP) in amyloid formation in vitro. J Mol Biol 287:781–796

Knight JD, Miranker AD (2004) Phospholipid catalysis of diabetic amyloid assembly. J Mol Biol 341:1175–1187

Konarkowska B, Aitken JF, Kistler J, Zhang SP, Cooper GJS (2006) The aggregation potential of human amylin determines its cytotoxicity towards islet beta-cells. Febs J 273:3614–3624

Lazaridis T (2003) Effective energy function for proteins in lipid membranes. Proteins 52:176–192

Lazaridis T, Karplus M (1999a) Discrimination of the native from misfolded protein models with an energy function including implicit solvation. J Mol Biol 288:477–487

Lazaridis T, Karplus M (1999b) Effective energy function for proteins in solution. Proteins 35:133–152

Macdonald RC, Macdonald RI, Menco BPM, Takeshita K, Subbarao NK, Hu LR (1991) Small-volume extrusion apparatus for preparation of large, unilamellar vesicles. Biochim Biophys Acta 1061:297–303

Martins IC, Kuperstein I, Wilkinson H, Maes E, Vanbrabant M, Jonckheere W, Van Gelder P, Hartmann D, D'Hooge R, De Strooper B, Schymkowitz J, Rousseau F (2008) Lipids revert inert A beta amyloid fibrils to neurotoxic protofibrils that affect learning in mice. EMBO J 27:224–233

Matsuzaki K, Sugishita K-I, Ishibe N, Ueha M, Nakata S, Miyajima K, Epand RM (1998) Relationship of membrane curvature to the formation of pores by magainin2. Biochemistry 37:11856–11863

Mazor Y, Gilead S, Benhar I, Gazit E (2002) Identification and characterization of a novel molecular-recognition and self-assembly domain within the islet amyloid polypeptide. J Mol Biol 322:1013–1024

Nanga RPR, Brender JR, Xu JD, Veglia G, Ramamoorthy A (2008) Structures of rat and human islet amyloid polypeptide IAPP(1–19) in Micelles by NMR spectroscopy. Biochemistry 47:12689–12697

Nanga RPR, Brender JR, Xu JD, Hartman K, Subramanian V, Ramamoorthy A (2009) Three-dimensional structure and orientation of rat islet amyloid polypeptide protein in a membrane environment by solution NMR spectroscopy. J Am Chem Soc 131:8252–8261

Neria E, Fischer S, Karplus M (1996) Simulation of activation free energies in molecular systems. J Chem Phys 105:1902–1921

Nilsson MR, Raleigh DP (1999) Analysis of amylin cleavage products provides new insights into the amyloidogenic region of human amylin. J Mol Biol 294:1375–1385

Ramamoorthy A, Thennarasu S, Lee D-K, Tan A, Maloy L (2006) Solid-State NMR investigation of the membrane-disrupting mechanism of antimicrobial peptides MSI-78 and MSI-594 derived from magainin 2 and melittin. Biophys J 91:206–216

Reches M, Porat Y, Gazit E (2002) Amyloid fibril formation by pentapeptide and tetrapeptide fragments of human calcitonin. J Biol Chem 277:35475–35480

Sciacca MFM, Pappalardo M, Milardi D, Grasso DM, La Rosa C (2008) Calcium-activated membrane interaction of the islet amyloid polypeptide: Implications in the pathogenesis of type II diabetes mellitus. Arch Biochem Biophys 477:291–298

Sciacca MFM, Pappalardo M, Attanasio F, Milardi D, La Rosa C, Grasso DM (2010) Are fibril growth and membrane damage linked processes? An experimental and computational study of IAPP(12–18) and IAPP(21–27) peptides. New J Chem 34:200–207

Scrocchi LA, Ha K, Chen Y, Wu L, Wang F, Fraser PE (2003) Identification of minimal peptide sequences in the (8–20) domain of human islet amyloid polypeptide involved in fibrillogenesis. J Struct Biol 141:218–227

Smith CK, Regan L (1997) Construction and design of β-sheets. Acc Chem Res 30:153–161

Smith PES, Brender JR, Durr UHN, Mullen DG, Banaszak Holl MM, Ramamoorthy A (2010) Solid-state NMR reveals the hydrophobic-core location of poly(amidoamine) dendrimers in biomembranes. J Am Chem Soc 132:8087–8097

Soong R, Brender JR, Macdonald PM, Rmamoorthy A (2009) Association of highly compact type II diabetes related islet amyloid polypeptide intermediate species at physiological temperature revealed by diffusion NMR spectroscopy. J Am Chem Soc 131:7079–7085

Tenidis K, Waldner M, Bernhagen J, Fischle W, Bergmann M, Weber M, Merkle ML, Voelter W, Brunner H, Kapurniotu A (2000) Identification of a penta- and hexapeptide of islet amyloid polypeptide (IAPP) with amyloidogenic and cytotoxic properties. J Mol Biol 295:1055–1071

Tracz SM, Abedini A, Driscoll M, Raleigh DP (2004) Role of aromatic interactions in amyloid formation by peptides derived from human amylin. Biochemistry 43:15901–15908

Westermark P, Wernstedt C, Wilander E, Sletten K (1986) A novel peptide in the calcitonin gene related peptide family as an amyloid fibril protein in the endocrine pancreas. Biochem Biophys Res Commun 140:827–831

Westermark P, Wernstedt C, O'brien T, Hayden D, Johnson K (1987a) Islet amyloid in type-2 diabetes mellitus and adult diabetic cats contain a novel putative polypeptide hormone. Am J Physiol 127:414–417

Westermark P, Wernstedt C, Wilander E, Hayden D, O'brien T, Johnson K (1987b) Amyloid fibrils in human insulinoma and islets of Langerhans of the diabetic cat are derived from neuropeptide-like protein also present in normal islets. Proc Natl Acad Sci USA 84:3881–3885

Westermark P, Wilander E, Westermark GT, Johnson KH (1987c) Islet amyloid polypeptide-like immunoreactivity in the islet B cells of Type 2 (non-insulin-dependent) diabetic and non-diabetic individuals. Diabetologia 30:887–892

Williams RW, Chang A, Juretic D, Loughran S (1987) Secondary structure predictions and medium range interactions. Biochim Biophys Acta 916:200–204

Wimley WC, White SH (1996) Experimentally determined hydrophobicity scale for proteins at membrane interfaces. Nat Struct Biol 3:842–848